



## Ignition and combustion of mechanically alloyed Al–Mg powders with customized particle sizes

Yasmine Aly, Mirko Schoenitz, Edward L. Dreizin \*

Otto H. York Department of Chemical, Biological, and Pharmaceutical Engineering, New Jersey Institute of Technology, Newark, NJ 07102, United States

### ARTICLE INFO

#### Article history:

Received 9 October 2012  
Received in revised form 21 December 2012  
Accepted 26 December 2012  
Available online 25 January 2013

#### Keywords:

Metal combustion  
Alloys  
Particle combustion  
Laser ignition  
Aerosol combustion

### ABSTRACT

Adding aluminum to propellants, pyrotechnics, and explosives is common to boost their energy density. A number of approaches have been investigated that could shorten aluminum ignition delay, increase combustion rate, and decrease the tendency of aluminum droplets to agglomerate. Previous work showed that particles of mechanically alloyed Al–Mg powders burn faster than similarly sized particles of pure aluminum. However, preparation of mechanically alloyed powders with particle sizes matching those of fine aluminum used in energetic formulations was not achieved. This work is focused on preparation of mechanically alloyed, composite Al–Mg powders in which both internal structures and particle size distributions are adjusted. Milling protocol is optimized to prepare equiaxial, micron-scale particles suitable for laboratory evaluations of their oxidation, ignition, and combustion characteristics. Oxidation of the prepared powders is studied using thermo-analytical measurements. Ignition is characterized experimentally using an electrically heated filament setup. Combustion is studied using a constant volume explosion setup for the powder cloud combustion, and a laser ignition setup for characterization of combustion rates and temperatures for individual particles. For the prepared materials, ignition and combustion characteristics are compared to those of pure Al. It is observed that the mechanically alloyed powders ignite at much lower temperatures than Al. Once ignited, the particles burn nearly as fast as Al, resulting in an overall improvement of the combustion performance.

© 2013 The Combustion Institute. Published by Elsevier Inc. All rights reserved.

### 1. Introduction

Metal-based, binary, mechanically alloyed and nanocomposite materials offer advantageous performance as fuel additives in energetic formulations for propellants, explosives, and pyrotechnics [1–5]. Recent research is focused on aluminum-based materials with reactivity enhanced compared to pure Al powders. These materials have high combustion enthalpies (typical of Al), with tailored density, high energy density, and reduced ignition delays (i.e., alloys or composites of Al–Mg, Al–Ti, etc.) [6–11]. In addition, research was active to produce nano-sized powders of reactive metals [12–14], which achieve high burn rates due to highly developed reactive surface [15]. New materials prepared by arrested reactive milling [16] combine advantages of conventional, micron-sized composite or alloyed powders with reactivity of energetic nanomaterials [7,17–21]. In order for these materials to be practically useful, their particle size distribution should be adjusted to make them compatible with the existing protocols for preparation of energetic formulations. However, cold welding that often occurs due to the ductile nature of Al prevents synthesis

of mechanically alloyed powders with useful size distributions. Process control agents (PCAs) have been used previously to avoid or minimize cold welding; similarly, smaller particle sizes can, in principle, be obtained by using smaller milling balls [22]. However, Al-based mechanically alloyed powders with attractive compositions prepared to date [9,23] were too coarse for practical applications. Long milling durations and increased PCA amounts can be used to further reduce particle size, but milling tools and PCAs contaminate the desired formulations [22].

This paper discusses the preparation and characterization of mechanically alloyed Al–Mg powders with customized particle size distributions. Al–Mg alloys have been explored for applications in energetic materials for a long time. Some of the first applications were in pyrotechnic formulations [24–26] while more recently, such alloys were successfully added to propellants [27]. It has been reported that Al–Mg alloys ignite at much lower temperatures than pure Al [28,29]. Combustion of alloys was also studied, with most detailed experimental observations on coarse particles with dimensions exceeding 100  $\mu\text{m}$  [30–32]. It was reported that depending on composition, either Al or Mg determine the alloy combustion dynamics [33]; alternatively, a staged combustion behavior was described, in which Mg combustion preceded that of Al [34]. Despite significant attention to combustion

\* Corresponding author. Fax: +1 973 642 4282.  
E-mail address: [dreizin@njit.edu](mailto:dreizin@njit.edu) (E.L. Dreizin).

characteristics of Al–Mg alloys [31,35,36], combustion of fine particles of such alloys has not been studied in detail, most likely because such fine particles are not readily available. Thus, enabling preparation of fine Al–Mg alloy powders by mechanical alloying, a very versatile materials manufacturing method, is of substantial interest. The issue is challenging primarily due to high ductility of Al, which tends to result in cold welding and coarse product particles. In previous research, elemental iodine was milled with aluminum resulting in particle size reduction [37]. In this work, iodine is used as an additional PCA enabling a better control over the particle shapes and sizes for an Al–Mg alloy. A 2-step ball milling technique is implemented with the first milling step used to achieve the desired structural and compositional refinement. Iodine is added and smaller milling balls are used for the second milling step aimed to reduce particle sizes. Combustion and ignition of the prepared materials is investigated and correlations between different oxidation, ignition, and combustion characteristics are studied.

## 2. Experimental

### 2.1. Material synthesis

Starting materials included elemental powders of Al (Atlantic Equipment Engineers, 99.8% pure, –325 mesh) and Mg (Alfa-Aesar, 99.8% pure, –325 mesh). Powders were blended and mechanically milled using a Retsch PM-400 MA planetary mill. Nominal powder composition was  $\text{Al}_{0.47}\text{Mg}_{0.53}$ , or 1:1 for Al:Mg by weight. The rotational speed was set to 350 rpm. The direction of rotation was set to reverse every 15 min.

The powders were milled in two steps. The first step was aimed to achieve compositional homogeneity between components as in conventional mechanical alloying. The second step was added to tailor the particle size distributions of the produced powders using additional PCA and altered milling conditions. The powder prepared in the two-step (2-step) milling was compared to a reference mechanically alloyed sample prepared in one step (1-step) with a duration equal to the total milling time of the 2-step procedure. Additional comparisons were made with the powder prepared using only the first step (1st step) of the 2-step procedure.

For the 1st step milling, elemental powders of Al and Mg were loaded in 0.5-l steel milling vials with 9.5-mm diameter hardened steel milling balls. Vials were filled in argon with a 30-g powder load and 300 g of milling balls (charge ratio of 10). 50 ml of hexane ( $\text{C}_6\text{H}_{14}$ ) was added to each milling vial as a PCA. The milling duration was 120 min. This completed the 1st step milling. For further processing, vials were opened in argon and iodine ( $\text{I}_2$ , chips, Sigma Aldrich, 99% pure) was added as 4 wt.% of the initial powder load to serve as a new PCA. After adding iodine, the vials were closed and milled for 5 min. to clean the 9.5-mm milling balls, which were then removed and replaced with the same mass of 3-mm diameter steel milling balls. The balls were replaced inside an Ar-filled glovebox. The second, softer milling step was then performed to produce mechanically alloyed powder with the desired finer particle sizes. The duration of the second milling step was 60 min. The total milling time was, therefore, 185 min. This milling time was also used to prepare reference samples milled in a 1-step process. Other milling conditions corresponded to those used in the first step of the 2-step milling, while iodine (4 wt.%) was included with the starting blend of Al and Mg powders.

The prepared powders were removed from the milling vials in the Ar-filled glovebox. The powder was left in the glovebox overnight, where it was exposed to an environment with low oxygen concentration (~2%). This exposure passivated the powder surface so that the powder could then be recovered and handled in open air.

### 2.2. Material characterization

Scanning electron microscopy (SEM) was used to study powder morphology using a Phenom Tabletop Microscope by FEI Technologies Inc. Backscattered electron images were taken to inspect particle shapes and sizes. Particle size distributions of the prepared composites were measured with low-angle laser light scattering using a Beckman-Coulter LS230 Enhanced Particle Analyzer. Powder suspensions for analysis were prepared in ethylene glycol ( $\text{C}_2\text{H}_6\text{O}_2$ ) and sonicated to minimize particle agglomeration. Phase compositions of the samples were analyzed using X-ray Diffraction (XRD) on a Phillips X'pert MRD powder diffractometer operated at 45 kV and 40 mA, using Cu  $K\alpha$  radiation ( $\lambda = 1.5438 \text{ \AA}$ ). The patterns were collected between  $10^\circ$  and  $85^\circ$  at a rate of  $0.625^\circ/\text{min}$ .

Thermal stability and temperature-dependent phase transformations were studied using differential scanning calorimetry (DSC) and thermogravimetric analysis (TGA) using a Netzsch Simultaneous Thermal Analyzer STA409 PG with a DSC sample carrier and corundum sample crucibles. Oxidation experiments were performed in a mixed 1:1 ratio of oxygen (50 ml/min, Matheson, 99.98% purity) and ultra-high purity argon (50 ml/min, Matheson, 99.99%) at various heating rates between 5 and 40 K/min. Decomposition experiments were performed in argon only and at a heating rate of 5 K/min. Ignition of the prepared materials was analyzed using a heated filament ignition apparatus described in detail elsewhere [38,39]. A thin layer of powder was coated onto a nickel–chromium alloy wire (manufacturer-specified working temperature range up to 1953 K). The wire was heated by a DC current and its temperature was monitored optically using an infrared pyrometer focused on its uncoated surface adjacent to the powder coating. Concurrently, light emission from the powder coating was measured using a photodiode sensor, in which a sharp onset of light emission was identified as the ignition instant. The temperature measured by the pyrometer at that instant was assumed to be the ignition temperature. Such experiments were conducted in air for a range of heating rates between  $10^3$  and  $10^5$  K/s. Ignition instant was also identified from videos recorded using a high-speed camera (MotionPro500 by Redlake) at 500 fps.

Combustion was studied using a constant volume explosion (CVE) setup for powder aerosol combustion, and a laser ignition setup for characterization of combustion rates and temperatures for individual particles. The details of the CVE experiments were described elsewhere [40–42]. The aerosolized powders were ignited from the center of a nearly spherical 9.2-L vessel. The vessel was initially evacuated, after which the powder was introduced with an air blast by opening a solenoid valve connecting the vessel with a chamber filled with compressed air. After the air blast, ignition was triggered following a delay of 300 ms, provided to reduce turbulence. The targeted initial pressure in the explosion vessel prior to ignition was 1 atm. Combustion pressure traces were recorded using both static and dynamic transducers. The measured pressure traces are normalized by the initial pressure in the vessel ( $P/P_0$ ). The rates of pressure rise,  $d(P/P_0)/dt$ , are also reported for the prepared composite and reference pure Al powder. ( $P/P_0$ ) and  $d(P/P_0)/dt$  are proportional to the flame temperature and combustion reaction rate, respectively [43].

For laser-ignited single particle combustion, the experimental technique is described in Refs. [44–46]. A vertically rising particle jet with low number density was generated using a vibratory powder feeder [47]. Particles ignited when crossing a  $\text{CO}_2$  laser beam. Luminous streaks produced by the ignited particles were photographed. Four photomultiplier tubes (PMT, Hamamatsu H3164-10) were used to record the light emission from burning particles. The PMTs were equipped with interference filters (486, 532, 568, and 589 nm). Emission signals filtered at 532 and 589 nm were used for optical pyrometry. The 486 nm filter was

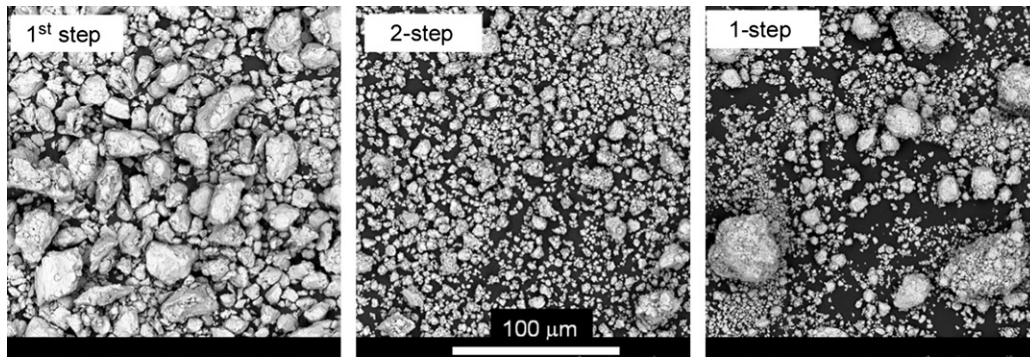


**Fig. 1.** SEM images of Al-Mg powders: the product of the 1st, 120-min. milling step (left); the product of the 2-step milling, total time 185 min. (center), and product of the 1-step milling, total time 185 min. (right).

selected to track one of the strongest AlO emission bands as an indicator of the intensity of the vapor-phase reactions. Because no substantial AlO emission occurs at 568 nm, the strength of the observed AlO emission was evaluated using the ratio of the signal intensities measured at 486 and 568 nm:  $R_{\text{AlO}} = I_{486}/I_{568}$ . Following Ref. [48], the measured ratio was normalized by its theoretical value calculated for respective intensities of a black-body emitter at the same temperature as the measured particle temperature.

### 3. Results

#### 3.1. Particle sizes, morphology, and phase composition

Figure 1 shows SEM images of the prepared powders. The image on the left shows the coarse powder obtained after the first, 120-min milling step. This milling time was selected based on the SEM images of the product showing equiaxial particles rather than flakes, with no apparent compositional contrast between Al and Mg (clearly visible at shorter milling times), and with no apparent detached Al or Mg particles. The powder prepared during the 1st milling step has a mean volumetric size of  $\sim 23 \mu\text{m}$ , as seen in Fig. 2. The product of the 2-step milling is shown in the center image of Fig. 1. The powder includes fine, equiaxial particles with

rounded shapes and a narrow size distribution (Fig. 2). The reduction in the mean volumetric particle size (from 23 to  $12.5 \mu\text{m}$ , cf. Fig. 2) caused by the second milling step is also apparent in Fig. 1. To further validate the effectiveness of this modified, 2-step milling procedure, the powder was compared to a reference sample prepared in 1-step with the same milling time as the 2-step sequence, as shown in the right most image of Fig. 1. The particles of the reference sample appear to have a broader size distribution compared to the powder prepared using the 2-step process. This is also apparent in the size distribution measurements in Fig. 2. The 1-step powder is coarser and has a broader particle size distribution than the powder prepared by the 2-step milling, despite a similar volumetric mean.

Figure 3 shows XRD patterns for the 1st step (120 min.) and 2-step (185 min.) milled powders as well as for a blended Al-Mg sample used as a reference. Peaks corresponding to pure Al and Mg are indicated in the plot. Remaining peaks have been identified as the  $\gamma\text{-Al}_{12}\text{Mg}_{17}$  intermetallic. For the 1st step powder, the pattern shows that peaks of Al and Mg are present along with peaks corresponding to  $\gamma\text{-Al}_{12}\text{Mg}_{17}$ . For the 2-step powder, the pattern shows that all Mg is incorporated into  $\text{Al}_{12}\text{Mg}_{17}$  phase mixed with the little remaining pure Al. The XRD pattern of the 2-step milled powder matches well the patterns for mechanically-alloyed Al-Mg powders reported previously [23].

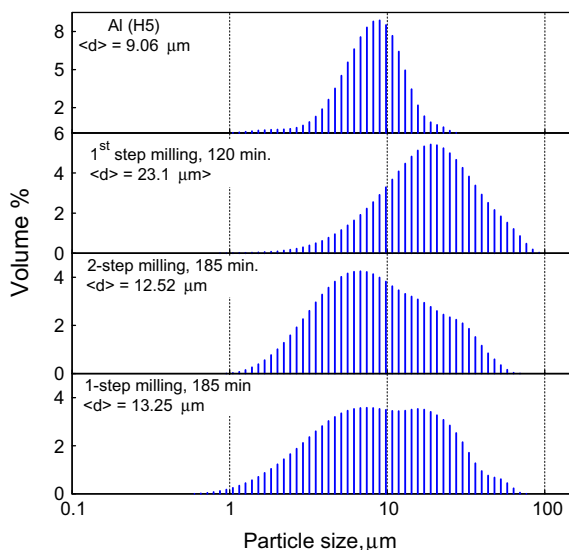


**Fig. 2.** Particle size distributions of the products of the first milling step (120 min.), 2-step milling (185 min.), 1-step milling (185 min.), and pure Al powder (top) used as a reference in aerosol combustion experiments. Volume mean particle sizes are shown for each powder.

#### 3.2. Ignition

Figure 4 shows the ignition temperatures of the prepared Al-Mg powders as a function of heating rate, with each point representing an individual ignition experiment. As expected for a thermally

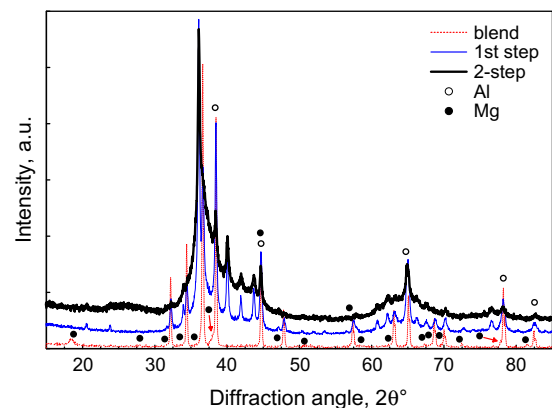


**Fig. 3.** XRD patterns of an Al-Mg blend, 1st step (120 min.), and 2-step (185 min.) milled powders. Elemental Al and Mg phases are indicated in the plot. All other (unlabeled) peaks correspond to the  $\gamma\text{-Al}_{12}\text{Mg}_{17}$  phase.

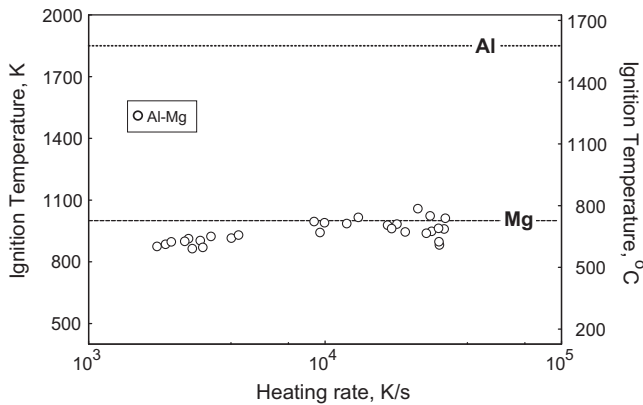


Fig. 4. Ignition temperatures of Al-Mg powders prepared by the 2-step milling as a function of heating rate.

activated ignition mechanism, ignition temperatures increase slightly with increasing heating rates. Ignition temperatures are approximately 860 K at lower heating rates and 1060 K for higher heating rates. These temperatures are somewhat higher than 783 K reported for an Al-Mg alloy with similar composition but ignited by its slow heating [28]. For comparison, ignition temperatures for pure Al and Mg powders are also shown. Ignition temperatures of Al-Mg composites are much lower than  $\sim 1850$  K reported for ignition of pure Al [49] at similar heating rates, and seem to be close to the ignition temperature of the pure Mg [39].

### 3.3. Thermal analysis and reaction kinetics

DSC and TGA traces for the decomposition experiments performed in Ar at 5 K/min are shown in Fig. 5. Poorly distinguished, intermetallic formation reactions can be observed at low temperatures in DSC. A weak exothermic feature is seen where sub-solidus reactions are expected compared to more detailed earlier measurements for the mechanically alloyed Al-Mg powders [23,50]. An endothermic peak corresponding to the eutectic melting at  $\sim 450$  °C ( $\sim 723$  K) is visible for both powders and occurs as expected from the binary Al-Mg phase diagram [50,51]. At higher temperatures (after eutectic melting), poorly resolved exothermic

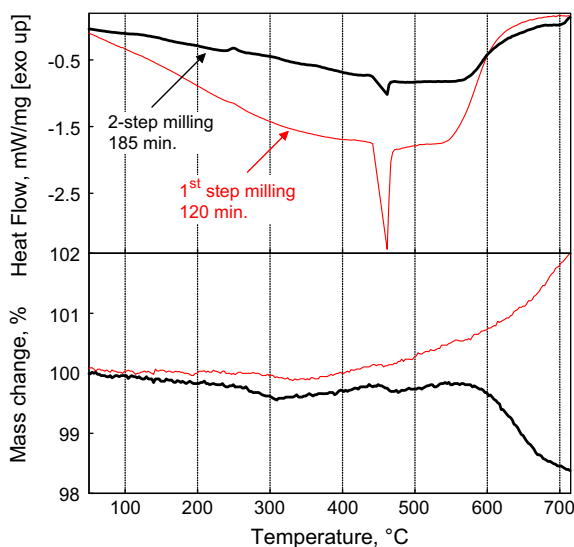


Fig. 5. DSC and TGA traces for the decomposition experiments performed in Ar at 5 K/min for 1st and 2-step milled Al-Mg powders.

features in DSC are observed and may be attributed to oxidation involving oxygen impurity in the flowing Ar gas environment. This oxidation results in a mass increase of about 2% recorded by TGA for the 1st step milled powder. For the 2-step powder, the mass loss of  $\sim 2\%$  occurring after eutectic melting is attributed to the release of  $I_2$ , similar to the  $I_2$  release observed in mechanically milled Al- $I_2$  powders [48]. Assuming that the 2-step powder oxidizes similarly to the 1st step powder, it is reasonable to conclude that the entire iodine introduced during milling, i.e., 4 wt.% of the powder mass, is retained in the 2-step powder as prepared.

Figure 6 shows DSC and TGA traces for the Al-Mg powders prepared by 1- and 2-step milling, as well as powder prepared by the 1st step milling heated in the mixed  $O_2/Ar$  environment. For all traces, an endotherm corresponding to that of the eutectic melting at  $\sim 450$  °C is observed [9,23,50–52]. An exotherm corresponding to the strong oxidation step in TGA is also observed consistently for all materials. For the composite prepared using the 2-step milling, the oxidation has an earlier onset than for the other samples. Both samples milled for 185 min (using both 1- and 2-step milling protocols) show exothermic peaks immediately after the eutectic melting. This post-eutectic melting exotherm is not present in the 1st step milled sample. The oxidation behavior described in Ref. [52] for Al-Mg composites with a comparable composition is qualitatively similar to that observed for the latter (1st step) sample prepared in this project.

The powder prepared using the 2-step procedure was heated in TGA in the same oxidative environment at different heating rates in the range of 5–40 K/min. Derivatives of TGA traces (DTG) at varying heating rates were used to construct Kissinger plots [53] using the DTG peak maxima. The resulting Kissinger plot (logarithm of heating rate,  $\beta$ , divided by temperature square vs. inverse temperature) is shown in Fig. 7; it also shows the results of the filament ignition experiments presented in Fig. 4. From Fig. 7, it is apparent that the points corresponding to the strong oxidation step do not line up with those of the filament ignition. This indicates that relatively strong exothermic processes detected in thermo-analytical measurements do not directly cause ignition of these powders. Further, one must consider that the measured filament ignition temperatures recorded are those of the filament and not of the powder coating, suggesting that the points seen in Fig. 7 could shift more to the right side of the plot, if corrected to

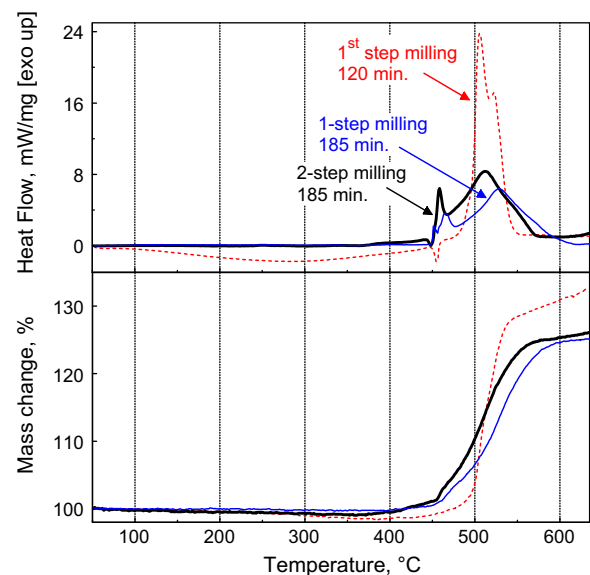


Fig. 6. DSC traces for Al-Mg powders heated in oxygen at 5 K/min prepared using different milling procedures, including 1st step, 2-step, and 1-step milling.

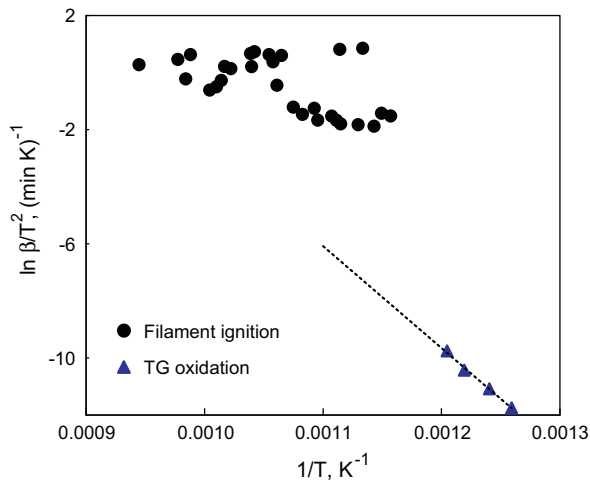


Fig. 7. Kissinger plot comparing ignition and oxidation data for Al-Mg composites as a function of heating rate.

represent the actual powder temperature. Considering such a correction, it would appear that an event occurring at a lower-temperature (perhaps eutectic melting or formation of an intermetallic phase) may lead to ignition, e.g., by generating additional fresh surface in the sample.

#### 3.4. Powder cloud combustion

Both 1- and 2-step milled Al-Mg powders and reference Al (H5 powder by Valimet) powder were tested in the CVE experiment using the same initial powder mass loadings of 4.65 g (corresponding to a fuel-rich mixture in the vessel). Results of these experiments are shown in Fig. 8. The Al-Mg powder prepared using the 2-step milling technique has the highest pressure output and shortest ignition delay as compared to both the reference H5 Al and Al-Mg powder prepared by 1-step milling. A better performance of the 2-step milled powder as compared to the 1-step milled powder may be due to a narrower particle size distribution (cf. Fig. 2), with fewer coarse particles hindering the reaction.

Table 2.1 summarizes the mean pressure and rate of maximum pressure rise ratio values for the prepared Al-Mg and reference H5 Al powder. Standard deviation values were calculated from repeated experiments. Al-Mg powders show higher  $(P/P_0)_{\max}$  and  $[d(P/P_0)/dt]_{\max}$  values than pure Al powder, indicating a higher flame temperature and combustion rate. For reference, explosion pressures calculated for the constant volume combustion using

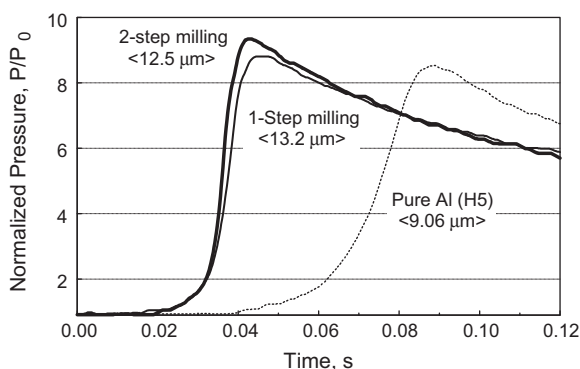


Fig. 8. Normalized pressure as a function of time for 2-step (185 min.), single-step, and reference Al samples.

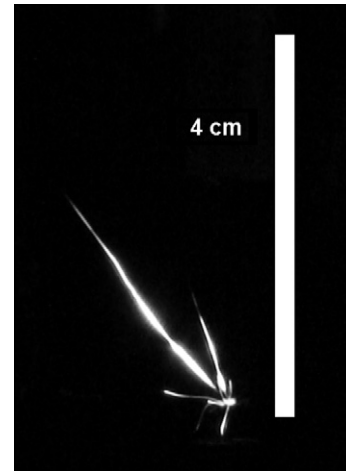


Fig. 9. Burning particle streaks of Al-Mg powder prepared following the 2-step milling process and ignited in the CO<sub>2</sub> laser beam.

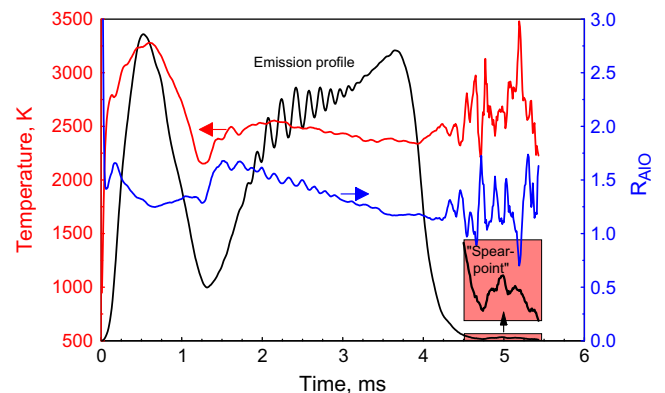


Fig. 10. Emission signal (vertical scale is in arbitrary units, the axis is not shown), temperature, and an intensity ratio characterizing significance of the molecular AlO emission for a single laser-ignited particle of mechanically alloyed Al-Mg powder prepared following the 2-step procedure (185 min. milling time).

Table 2.1

Summary of CVE experiment results (data represent average values  $\pm$  standard deviations).

Sample	$(P/P_0)_{\max}$	$[d(P/P_0)/dt]_{\max}$ ( $s^{-1}$ )	$(P/P_0)_{\max}$ calculated
Al-Mg (2-step)	$9.02 \pm 0.28$	$1135 \pm 207$	13.3
Al-Mg (1-step)	$8.89 \pm 0.49$	$1061 \pm 166$	13.3
Pure Al (H5)	$8.54 \pm 0.33$	$439 \pm 105$	12.4

experimental powder loads in air are also shown in Table 2.1. The calculations used NASA CEA code [54] and Al-Mg alloys were treated as blended Al and Mg powders. Initial pressure was assumed to be 1 atm and the reactants were taken at room temperature. The comparison of calculated and experimental pressures shows that the experimental pressures are systematically lower than the pressures predicted by the thermodynamic equilibrium for all materials, as expected because of incomplete combustion and heat losses.

#### 3.5. Single particle combustion

A photograph of burning particle streaks is shown in Fig. 9 for the Al-Mg powder prepared by the 2-step milling. Several particle streaks observed in Fig. 9 were produced by different particles fed

successively through the laser beam during the time of exposure. Each well discerned streak represents a particle passing through the CO<sub>2</sub> laser beam. Most streaks include two separate bright portions and end with characteristic spearpoints.

A typical emission trace, a temperature trace obtained by 2-color pyrometry, and a ratio  $R_{\text{AlO}}$  for a burning Al-Mg particle are shown in Fig. 10. Consistently with the visible streaks in Fig. 9, emission traces in Fig. 10 also show distinct peaks. The first peak corresponds to a higher temperature and lower level of AlO emission. The initial temperature increase is consistent with the emission intensity ramp. The first peak is then followed by a second peak accompanied with a characteristic oscillatory emission pattern. This second peak is typically longer than the first one. The measured temperature and  $R_{\text{AlO}}$  are observed to slowly decrease until the final small peak (corresponding to a “spearpoint” in the photograph) is observed. The overall emission intensity level at which the spearpoints occur is substantially reduced compared to its peak value, so that both temperature and  $R_{\text{AlO}}$  measurements are no longer meaningful.

Slight delays in the ignition of Al-Mg particles can be observed in the photograph in Fig. 9, i.e., luminous streaks do not always originate from the same area where the CO<sub>2</sub> beam was focused. These delays made it impossible to process the experimental data following the procedure outlined and used in Refs. [44–47], where the size of each particle was evaluated based on the amplitude of a light-scattering pulse, generated when particles crossed a low-power auxiliary laser beam placed just under the CO<sub>2</sub> laser beam. The poorly reproducible ignition timing made it impossible to correlate the light scattering and emission pulses and to quantify the size of each ignited particle. Instead, a methodology described in Ref. [55] was used to obtain a correlation between burn times and particle sizes. The main assumption in this data processing is that the larger size particles burn longer. First, recorded emission pulses were preliminarily inspected to remove overlapping or closely spaced signals, which may not represent individual particle combustion events. Durations of the downselected pulses were then measured. The data on pulse durations representing burn times were logarithmically binned and correlated with the particle size distributions for the respective powders measured by Beckman-Coulter LS230 Enhanced Particle Analyzer. The volume-based particle size distributions shown in Fig. 2 were transformed into number-based, cumulative distributions, to be directly compared to the burn time data shown in Fig. 11. For reference, Fig. 11 also shows the burn times measured elsewhere for the reference Al 10–14 μm powder [44–47], binned the same way as the results of the present measurements for Al-Mg powders. Once the size distributions are obtained in terms of particle number densities in respective size bins, the data shown in Fig. 11 are recast in terms of particle burn times as a function of their size.

The particle size distributions are shown in Fig. 12 in terms of cumulative number density as a function of particle size. These cumulative number density curves (Fig. 12) were fitted using a log normal distribution function and correlated to the burn time. The final burn times as a function of particle sizes are shown in Fig. 13. For both powders, the result is well represented by  $t \sim d^n$  trends (shown as dashed lines). Burn times for Al-Mg particles greater than 2 μm are slightly longer than those of the same size pure Al particles; however, the difference is rather small.

The temperature and AlO emission signals, such as shown in Fig. 10, were averaged for each particle so that characteristic values could be assigned to the entire powder samples rather than individual particles. Average temperature values were calculated for each burn trace for the period of time when the emission signal varied within 50% and 100% of its peak value following the data processing described in [44–47]. The same procedure was used to calculate the average value of the normalized  $R_{\text{AlO}}$ . Resulting

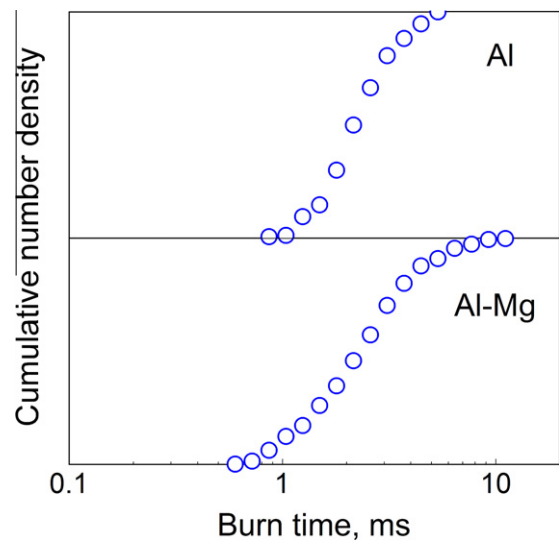


Fig. 11. Cumulative number density vs. burn time for Al-Mg powder particles prepared following the 2-step milling procedure and for pure Al powder (10–14 μm nominal particle size).

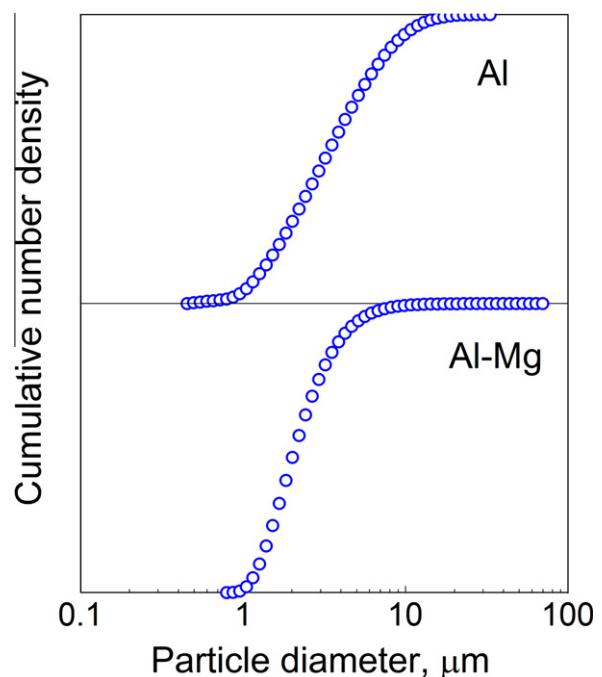
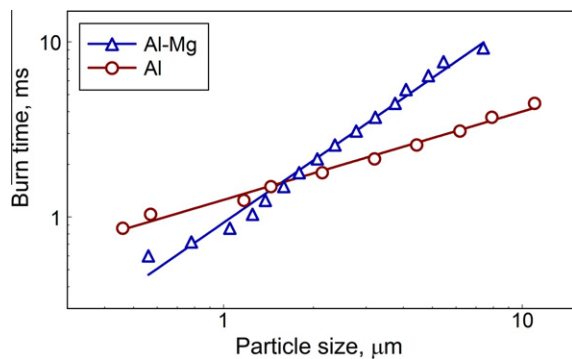
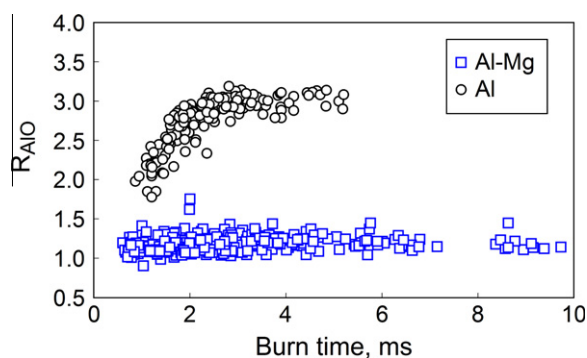


Fig. 12. Cumulative number density vs. particle size for Al-Mg powder particles prepared following the 2-step milling procedure and for pure Al powder.

average values of  $R_{\text{AlO}}$  and temperature are shown in Figs. 14 and 15, respectively. The data are shown for both the 2-step milled Al-Mg and pure Al powders. For Al combustion in air,  $R_{\text{AlO}}$  values greater than 1 indicate AlO vapor phase reactions. Values of  $R_{\text{AlO}}$  for Al-Mg powder are lower than those for pure Al, indicating substantial reduction in the importance of these vapor-phase reactions. Temperatures obtained for the Al-Mg powder are similar to those of pure Al. For both powders, despite substantial data scatter a slight increase in temperature is observed for particles with longer burn times. The increase in scatter in the calculated average temperatures for Al-Mg powder could be attributed to the morphology of the as-milled powders as well as the ignition delay observed in Fig. 9. Note that the emission signal changes



**Fig. 13.** Particle burn time as a function of size for the Al-Mg powder prepared using the 2-step milling and for pure Al powder. Lines show respective  $d^n$  fits ( $n \approx 0.5$  for Al and  $n \approx 1$  for the Al-Mg alloy).



**Fig. 14.** Normalized AIO ratio,  $R_{AIO}$ , values as a function of burn time for Al-Mg powder prepared using the 2-step milling and for pure Al powder.

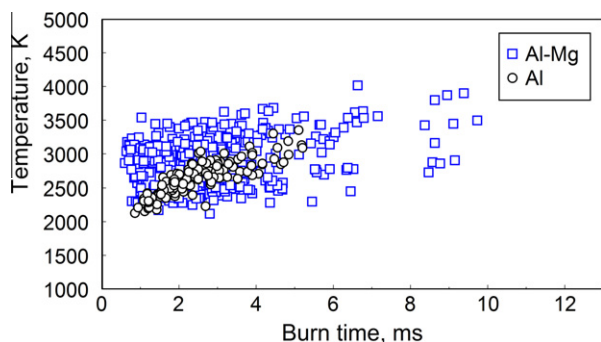


**Fig. 15.** Combustion temperature as a function of burn time for Al-Mg powder prepared using the 2-step milling and for pure Al powder.

noticeably during each particle combustion event, so that the average temperatures and  $R_{AIO}$  values provide only very approximate information on the related reaction mechanisms. A more detailed analysis of the burning particle temperature histories is of interest for future work.

#### 4. Discussion

Present experiments showed that iodine is a very effective PCA for mechanical alloying of Al-Mg powders. The powder particle sizes are reduced effectively (cf. Figs. 1 and 2) and with relatively short milling times. It is also shown that the 2-step milling offers a useful approach of tailoring particle sizes of mechanically alloyed powders without inducing substantial changes in their structure and causing their contamination by milling tools.

It was found that the initial nominal amount of  $I_2$  added to the powder is retained in the prepared materials (as detected by TGA, cf. Fig. 5). The effect of iodine on oxidation is not insignificant: the eutectic melting of Al-Mg alloys is immediately followed by substantial weight gain and energy release (Fig. 5) only for the materials prepared with added iodine. It is likely that iodine-coated (or iodide containing) layers separate nano-scale grains or are embedded between consolidated metal flakes. Iodine from these layers is likely released causing formation of fresh surface; such fresh surfaces oxidize readily causing the exotherm observed for these materials to follow the eutectic melting. It is likely that this phenomenon is also important for ignition of the prepared Al-Mg alloys.

Added iodine may have another side benefit for the reactive materials, resulting in formation of halogenated combustion products with biocidal properties. Such products are desired for applications aimed to improve inactivation of aerosolized spores and bacteria in a blast [56–59].

Ignition temperatures for the prepared 2-step powders vary from approximately 860 to 1060 K for the range of heating rates covered in the present ignition experiments. These temperatures are lower than the ignition temperatures reported for pure Al and close to those of pure Mg powders. Similar filament ignition experiments for mechanically alloyed Al-Mg powders reported previously [9] showed ignition temperatures of  $\sim 1020$  K which are only slightly higher than the ignition temperatures reported here. The slight decrease in temperatures could be due to the morphological and particle size differences in the powders. The powders prepared in this work are finer and have a smoother surface than those described previously [9].

CVE results are generally consistent with a previous report of faster burn of Al-Mg alloys [9]. An improvement in both maximum pressure and rate of pressure rise for the prepared alloys as compared to the reference pure Al powder is significant in terms of possible practical applications of the developed material. The present work also offers a more detailed characterization of particle combustion. Results of the laser ignition experiments show that once ignited, Al particles burn faster than similarly sized particles of Al-Mg alloys. This is in agreement with recent measurements comparing combustion rates of Al and other materials [47]. An improvement in the pressure traces measured in CVE, as well as accelerated burn reported earlier based on aerosol combustion experiments [9,60] are likely caused by a combination of the lowered ignition temperature and nearly unchanged burn rate.

The combustion mechanism of the prepared Al-Mg powders is clarified from the streaks and traces shown in Figs. 9 and 10, respectively. A two-peak structure of the emission pulse suggests a 2-staged burn. Consistently with the earlier observations and proposed reaction mechanisms [34], it is suggested that Mg selectively burns first (stage I) followed by combustion of Al (stage II). This suggestion is supported by a lower level of AIO emission during the initial portion of the emission pulse, corresponding to stage I. It is further supported by a characteristic oscillatory pattern observed during the stage II and common for Al particle combustion. This selective combustion of Mg is likely due to a lower vapor pressure of Mg compared to Al, enabling Mg vapors to react with surrounding air and consume all available oxygen, effectively starving Al combustion until Mg is consumed.

It is also interesting to compare the trends observed for particle burn times as a function of their diameter obtained in this work with similar trends reported previously. The same data set used to generate the trend reported in Fig. 13 for pure Al was processed previously to report a somewhat weaker effect of particle diameters on their burn times [44,45,61]. The discrepancy with the present interpretation shown in Fig. 13 is clearly attributed to the method used to process experimental data. When particle

sizes were measured independently of their burn times [44,45,61], the results implied that at least for some particles, smaller particles burn longer than larger ones. Such data points, likely indicative of errors associated either with particle size measurement or with matching emission and scatter pulses, were processed differently in the present experiments. While real-time particle size measurements were not used, the particle size distribution that was used to process the present data was obtained by a much more accurate measurement. The stronger effect of particle sizes on their burn times obtained here, i.e.,  $t \sim d^{0.5}$  for Al and  $t \sim d^1$  for Al-Mg alloy (rather than  $t \sim d^{0.3}$  reported previously for Al) appears to be more reasonable and amenable to a theoretical interpretation.

A slight increase in the average flame temperature with particle size for both Al-Mg and pure Al powders is likely associated with an increased importance of the stand-off vapor phase flame for larger particles. As discussed previously [62], the flame approaches the particle surface as the particle size decreases, eventually ceasing to exist for very fine particles. This changes the combustion regime from vapor-phase to surface reaction and is accompanied by reduction in the respective combustion temperature.

## 5. Conclusions

Preparation of mechanically alloyed powders of Al-Mg with fine particle sizes is feasible using a modified, 2-step milling technique that allows for simultaneous adjustment in both internal structures and particle size distributions. Particles suitable for laboratory evaluations of their oxidation, ignition, and combustion characteristics were prepared and characterized. Electron microscopy, X-ray diffraction patterns, and particle size distribution measurements showed that fine, equiaxial particles of Al-Mg with a homogeneous composition and a mean size of approximately 12.5  $\mu\text{m}$  were produced. Filament ignition experiments of these mechanically alloyed powders conducted in air showed ignition temperatures in the range of 860–1060 K, which is significantly lower than ignition temperatures reported for pure Al powders which ignite at around 1850 K. Premixed flames in air were produced in the powder cloud combustion experiments and showed that a higher pressure output and shorter ignition delay can be achieved as compared to pure Al powders. Single particle laser experiments showed that once ignited, Al-Mg particles burn nearly as fast as pure Al particles of the same dimensions. It is also observed that the Al-Mg particles burn in a two-stage process proposed to include selective combustion of Mg followed by combustion of Al. Despite the slightly longer burn times, the improved ignition of Al-Mg particles and their high combustion temperatures make them a viable replacement for pure Al powders in different energetic formulations.

## Acknowledgment

This work was supported by Defense Threat Reduction Agency.

## References

- [1] A. Gany, D.W. Netzer, *Int. J. Turbo Jet Engines* 2 (1985) 157–168.
- [2] B. Palaszewski, *J. Propul. Power* 8 (1992) 1192–1199.
- [3] B. Palaszewski, R. Powell, *J. Propul. Power* 10 (1994) 828–833.
- [4] J.K. Sambamurthi, E.W. Price, R.K. Sigman, *AIAA J.* 22 (1984) 1132–1138.
- [5] L. Meda, G. Marra, L. Galfetti, F. Severini, L. De Luca, *Mater. Sci. Eng., C* 27 (2007) 1393–1396.
- [6] E. Beloni, V.K. Hoffmann, E.L. Dreizin, *J. Propul. Power* 24 (2008) 1403–1411.
- [7] M. Schoenitz, T.S. Ward, E.L. Dreizin, *Proc. Combust. Inst.* (2005) 2071–2078.
- [8] Y.L. Shoshin, E.L. Dreizin, *Combust. Flame* 145 (2006) 714–722.
- [9] Y.L. Shoshin, R.S. Mudryy, E.L. Dreizin, *Combust. Flame* 128 (2002) 259–269.
- [10] D. Stamatidis, Z. Jiang, V.K. Hoffmann, M. Schoenitz, E.L. Dreizin, *Combust. Sci. Technol.* 181 (2009) 97–116.
- [11] X. Zhu, M. Schoenitz, E.L. Dreizin, *J. Alloys Compd.* 432 (2007) 111–115.
- [12] L. De Luca, L. Galfetti, F. Severini, L. Meda, G. Marra, A.B. Vorozhtsov, V.S. Sedoi, V.A. Babuk, *Combust. Explosion Shock Waves* 41 (2005) 680–692.
- [13] A. Pivkina, P. Ulyanova, Y. Frolov, S. Zavyalov, J. Schoonman, *Propellants, Explos., Pyrotech.* 29 (2004) 39–49.
- [14] P. Brousseau, C.J. Anderson, *Propellants, Explos., Pyrotech.* 27 (2002) 300–306.
- [15] A. Ingenito, C. Bruno, *J. Propul. Power* 20 (6) (2004) 1056–1063.
- [16] E.L. Dreizin, M. Schoenitz, US Patent 7,524,355, 2009.
- [17] E.L. Dreizin, *Prog. Energy Combust. Sci.* 35 (2009) 141–167.
- [18] M. Schoenitz, T.S. Ward, E.L. Dreizin, 43rd AIAA Aerospace Sciences Meeting, 2005, pp. 3001–3006.
- [19] S.M. Umbrajkar, M. Schoenitz, E. L. Dreizin, 45th AIAA Aerospace Sciences Meeting, 2007, pp. 3590–3595.
- [20] S.M. Umbrajkar, S. Seshadri, M. Schoenitz, V.K. Hoffmann, E.L. Dreizin, *J. Propul. Power* 24 (2) (2008) 192–198.
- [21] S. Umbrajkar, M.A. Trunov, M. Schoenitz, E.L. Dreizin, R. Broad, *Propellants, Explos., Pyrotech.* 32 (2007) 32–41.
- [22] C. Suryanarayana, *Prog. Mater. Sci.* 46 (2001) 1–184.
- [23] M. Schoenitz, E.L. Dreizin, *J. Mater. Res.* 18 (2003) 1827–1836.
- [24] J.H. O'Neill, US Patent 1532930, 1925.
- [25] J.H. de Boer, *Flash Lamp*, US Patent 2325667, 1943.
- [26] A.I. Sidorov, I.P. Kravchenko, V.M. Antonov, M.M. Arsh, F.P. Madyakin, L.Y. Gudoshnikova, S. Ugol'kova, Soviet Patent SU237041, 1969.
- [27] H. Habu, *Keikinzoku* 58 (2008) 162–166.
- [28] V.G. Poyarkov, *Izv. Vyssh. Ucheb. Zaved., Tsvet. Met.* 10 (1967) 149–153 (in Russian).
- [29] R.-H. Chen, C. Suryanarayana, M. Chaos, *Adv. Eng. Mater.* 8 (2006) 563–567.
- [30] E.I. Popov, L.Y. Kashporov, V.M. Mal'tsev, A.L. Breiter, *Fiz. Goreniya Vzryva* 9 (1973) 240–246.
- [31] A.L. Breiter, E.I. Popov, V.L. Velikanova, *Fiz. Aerodispersnykh Sist.* 23 (1983) 43–48 (in Russian).
- [32] A.A. Zenin, G.P. Kuznetsov, V.I. Kolesnikov, *Khim. Fiz.* 30 (2011) 28–41 (in Russian).
- [33] V.I. Glukhov, V.I. Gnatovskii, *Fiz. Aerodispersnykh Sist.* 5 (1971) 71–76 (in Russian).
- [34] E.I. Popov, L.Y. Kashporov, V.M. Mal'tsev, A.L. Breiter, *Combust. Explos. Shock Waves* 9 (2) (1975) 204–208.
- [35] S. Yuasa, T. Takeno, *Proc. Combust. Inst.* 19 (1982) 741–748.
- [36] T.A. Roberts, R.L. Burton, H. Krier, *Combust. Flame* 92 (1993) 125–143.
- [37] S. Zhang, M. Schoenitz, E.L. Dreizin, *J. Phys. Chem. Solids* 71 (2010) 1213–1220.
- [38] Y.L. Shoshin, M.A. Trunov, X. Zhu, M. Schoenitz, E.L. Dreizin, *Combust. Flame* 144 (2006) 688–697.
- [39] T.S. Ward, M.A. Trunov, M. Schoenitz, E.L. Dreizin, *Int. J. Heat Mass Transfer* 49 (2006) 4943–4954.
- [40] B.Z. Eapen, V.K. Hoffmann, M. Schoenitz, E.L. Dreizin, *Combust. Sci. Technol.* 176 (2004) 1055–1069.
- [41] P.R. Santhanam, V.K. Hoffmann, M.A. Trunov, E.L. Dreizin, *Combust. Sci. Technol.* 182 (2010) 904–921.
- [42] M. Schoenitz, E.L. Dreizin, E. Shtessel, *J. Propul. Power* 19 (2003) 405–412.
- [43] I. Glassman, *Combustion*, Academic Press, San Diego, CA, 1996.
- [44] C. Badiola, R.J. Gill, E.L. Dreizin, *Combust. Flame* 158 (2011) 2064–2070.
- [45] R.J. Gill, C. Badiola, E.L. Dreizin, *Combust. Flame* 157 (2010) 2015–2023.
- [46] R.J. Gill, S. Mohan, E.L. Dreizin, *Rev. Sci. Instrum.* 80 (2009).
- [47] E.L. Dreizin, C. Badiola, S. Zhang, Y. Aly, *Int. J. Energetic Mater. Chem. Propul.* (2012).
- [48] S. Zhang, C. Badiola, M. Schoenitz, E.L. Dreizin, *Combust. Flame* 159 (2012) 1980–1986.
- [49] S. Mohan, M.A. Trunov, E.L. Dreizin, *Proc. of 2003 Tech. Meeting of the Eastern States Section of the Combust. Inst.*, 2003, pp. 329–332.
- [50] D.L. Zhang, T.B. Massalski, M.R. Paruchuri, *Metall. Mater. Trans. A* 25 (1994) 73–79.
- [51] N. Saunders, *Calphad* 14 (1990) 61–70.
- [52] M. Schoenitz, E.L. Dreizin, *J. Propul. Power* 20 (2004) 1064–1068.
- [53] H.E. Kissinger, *Anal. Chem.* 29 (1957) 1702–1706.
- [54] B.J. McBride, S. Gordon, NASA RP 1311, 1996.
- [55] A. Corcoran, V.K. Hoffman, E.L. Dreizin, *Combust. Flame*, (2012) 718–724.
- [56] S.A. Grinshpun, A. Adhikari, M. Yermakov, T. Reponen, E.L. Dreizin, M. Schoenitz, V.K. Hoffmann, S. Zhang, *Environ. Sci. Technol.* 46 (2012) 7334–7341.
- [57] S. Zhang, M. Schoenitz, E.L. Dreizin, *J. Phys. Chem. C* 114 (2010) 19653–19659.
- [58] C. Farley, M.L. Pantoya, *J. Therm. Anal. Calorim.* 102 (2010) 609–613.
- [59] B.R. Clark, M.L. Pantoya, *Phys. Chem. Chem. Phys.* 12 (2010) 12653–12657.
- [60] E.L. Dreizin, Y.L. Shoshin, R.S. Mudryy, V.K. Hoffmann, *Combust. Flame* 130 (2002) 381–385.
- [61] C. Badiola, E.L. Dreizin, *Combust. Sci. Technol.* (2012).
- [62] S. Mohan, M.A. Trunov, E.L. Dreizin, *Combust. Flame* 156 (2009) 2213–2216.